An electrochemical and radiolytic study of the effects of H_2 on the corrosion of UO_2-based materials

Nazhen Liu [a,b,*], Fraser King [c], James J. Noël [a,d,*], David W. Shoesmith [a,d]

[a] Department of Chemistry, The University of Western Ontario, London, Ontario N6A 5B7, Canada
[b] Key Laboratory of Marine Environmental Corrosion and Bio-fouling, Institute of Oceanology, Chinese Academy of Sciences, Qingdao 266071, China
[c] Integrity Corrosion Consulting Ltd., Nanaimo, British Columbia V9T 1K2, Canada
[d] Surface Science Western, The University of Western Ontario, London, Ontario N6G 0J3, Canada

ABSTRACT

The influence of γ-radiation in the presence of dissolved hydrogen on the corrosion of uranium dioxide has been compared to the electrochemical behavior of uranium dioxide in aqueous chloride solutions. Hydrogen atoms, produced either electrochemically or by water radiolysis were shown to reduce U^V in the oxide leading to suppression of its corrosion. The removal of electrochemical polarization, and of hydrogen when γ-radiation was present, allowed re-oxidation of the uranium dioxide accompanied by the reformation of hydrogen. These results are consistent with published studies which show the corrosion of spent nuclear fuel can be suppressed in the presence of hydrogen. H_2 effect in suppressing the corrosion of UO_2-based materials without catalysis of noble metal particles is studied by producing H radicals electrochemically and radiolytically. Reactive H radicals produced by H_2O reduction at cathodic potentials, lead to the reduction of U^V states which are present due either to the Dy^{III} doping or the non-stoichiometry within the UO_2 based materials. When the cathodic potential is switched to open circuit, the relaxation of E_{CORR} (corrosion potential) indicates that the electrochemically reduced surface is unstable. The combination of γ-irradiation and H_2 can also lead to the reduction of UO_2. In the absence of dissolved H_2, a similar relaxation of E_{CORR} indicates that reactive H radicals produced electrochemically or radiolytically are responsible for the reduction of the UO_2 matrix.

1. Introduction

The universally accepted concept for the disposal of high level nuclear waste, in particular spent nuclear fuel (dominantly UO_2), is based on multiple barriers including the waste form, durable metal containers, a clay buffer and seals around the container, and a deep geologic repository (DGR) [1,2]. While such a DGR can provide acceptable assurance for long term containment, it is necessary to consider the consequences of container failure [3–6], which could lead to the exposure of fuel to the groundwater. Since the spent fuel contains the radioactive fission and activation products [7], its behavior in contact with groundwater provides the critical radioactivity source term in assessments of repository safety [8].

Since the groundwater entering the container will be anoxic, the dissolved O_2 having been consumed by reaction with organic matter, oxidizable minerals and container corrosion processes, the only source of oxidants inside a failed container will be those produced by H_2O radiolysis [9,10]. Since the solubility of the UO_2 fuel increases by many orders of magnitude when oxidized to U^{VI} (soluble as UO_2^{2+}) [11], radiolytic oxidants, in particular H_2O_2 [12], will lead to corrosion of the fuel and the release of radionuclides to the groundwater. The dependence of the fuel corrosion/dissolution rate on redox conditions is well established based on electrochemical studies and the measurement of corrosion rates (or rate constants) in the presence of oxidants and radiation fields [3,4,12–17].

However, the simultaneous corrosion of the carbon steel container by reaction with H_2O will produce the redox scavengers, Fe^{2+} and H_2, which will influence the redox conditions within the container via a number of homogeneous solution and heterogeneous surface reactions [6,14,18]. Of these two potential reducing agents, H_2 has been shown to be dominant in suppressing the corrosion rate of spent fuels, alpha doped UO_2, and SIMFUELS (UO_2 doped with non-radioactive elements to replicate the chemical effects of in-reactor irradiation [7]). Recent experimental [19] and modeling studies have shown that only

micromolar quantities of H_2 are required to suppress fuel corrosion [6, 9]. These observations have led to the proposal that natural uraninite deposits could be stabilized by the presence of radiolytically-produced H_2 in the deposit [20].

It has been demonstrated that H_2 cannot act as a homogeneous solution reductant [21], but must be activated; i.e., dissociated into reactive H atoms. It has been clearly demonstrated that activation can be achieved on SIMFUEL surfaces which contain segregated noble alloy (ε) particles [22–24], composed of Rh, Pd, Ru and Mo. With the exception of Mo, these metals are known to be exceptionally good catalysts for H_2 dissociation [25]. Since these particles are galvanically-coupled to the UO_2 matrix, they act as anodes which oxidize H atoms to produce protons forcing the matrix to adopt a potential too low to support its oxidation and dissolution. In the absence of these particles, this galvanic protection does not occur to any significant extent indicating that the activation of H_2 on a UO_2 surface is a minor process [23].

Some results suggest a major role for radiation, both alpha (α) and gamma (γ), by producing H atoms on the surface of UO_2 which can then scavenge radiolytic oxidants, such as H_2O_2, thereby suppressing UO_2 corrosion. This has been observed in a range of studies on α-doped UO_2, SIMFUELs (not containing noble metal elements) and α-irradiated UO_2 [10,19,22–24,26–29]. In the case of α-doped UO_2, the combination of H_2 and radiation also appeared to render the UO_2 surface unreactive even after the dissolved H_2 was subsequently removed [26]. Since, after the removal of H_2, radiolytic oxidants would no longer be scavenged, this suggests an irreversible response of the UO_2 surface to the combination of H_2 and radiation.

In this study, we investigated the response of UO_2 to γ radiation in the presence of dissolved H_2 and compared it to the electrochemical behavior of UO_2, since, at sufficiently negative applied potentials, the electrochemical reduction of H^+ is known to produce H atoms. Using electrochemical responses and a calibration curve for the relationship between the corrosion (open circuit) potential (E_{CORR}) and the composition of the surface determined by X-ray photoelectron spectroscopy (XPS), we have investigated the similarities in the responses of UO_2 to the reducing conditions produced electrochemically and in γ-irradiated solutions containing H_2.

2. Experimental

2.1. Experiments involving Dy_2O_3 doped UO_2 (Dy-UO_2) and non-stoichiometric $UO_{2.002}$

2.1.1. Electrode materials and preparation

The electrodes used in electrochemical experiments were UO_2 doped with 12.9 wt% Dy (Dy-UO_2) (resistivity = 280 Ω•cm) and a close-to-stoichiometric UO_2 specimen ($UO_{2.002}$) (resistivity > 10 kΩ•cm). The electrodes used in γ-irradiation experiments were cut from commercial UO_2 pellets (resistivity = 2.8 kΩ•cm). All materials were supplied by Canadian Nuclear Laboratories, Chalk River, ON, Canada. Since the resistivity of UO_2 is known to decrease with the extent of non-stoichiometry, as discussed elsewhere [30], the lower resistivity of the specimen used in radiation experiments compared to that of the close-to-stoichiometric $UO_{2.002}$, indicates incomplete reduction during sintering during the fuel fabrication process and a higher U^V content required to maintain charge balance in the oxide.

For electrochemical experiments, 2 mm-thick discs were cut from pellets and fabricated into electrodes using the previously published procedure [31] with the electrodes set in resin with only a single flat surface exposed to solution. The exposed surface area was 1.1 cm². The electrodes used in irradiation experiments were fabricated by a similar procedure but with the sides wrapped in PTFE tape leaving a surface area of 1.54 cm² exposed to solution [32].

2.1.2. Electrochemical equipment and procedures

Electrochemical experiments were performed in a standard three electrode cell. A commercial saturated calomel electrode (SCE (+0.242 V vs SHE)) was used, with a Pt foil spot welded to a Pt wire employed as the counter electrode. Potentials were controlled or measured, and current responses recorded, using a Solartron model 1287 potentiostat, with the current interrupt method employed to compensate for the electrode resistance. Corrware (Scribner Associates) was used to analyze data. Prior to an experiment, the exposed electrode surfaces were polished on wet 1200 grit SiC paper (600 grit in irradiation experiments), sonicated for 1 min, and rinsed in deionized H_2O.

In experiments involving cathodic pretreatments, a constant potential (E_{PRE}) between −1.2 V (vs SCE) and −1.5 V (vs SCE) was applied for 5 min. Subsequently, a number of different procedures were followed: (i) a potential of −0.6 V was applied and the current measured for 200 s; (ii) the potential was scanned to 0 V and back at a scan rate of 10 mV s^{-1}; (iii) the electrode was switched to open circuit and E_{CORR} recorded for ~ 40 h.

2.1.3. Solution preparation

Experiments were conducted in a 0.1 mol L^{-1} NaCl solution, with or without HCO_3^-, prepared with deionized H_2O (resistance 18.2 MΩ cm) obtained with a Millipore Milli-Q plus unit. The pH was adjusted using either NaOH or HCl (Caledon). All experiments were Ar-purged (ultra-high purity, Praxair) and conducted at room temperature. For solutions containing 0.001 mol L^{-1} NaHCO_3 (Caledon), the pH was 8.0.

2.2. Electrochemistry in the presence of gamma (γ) radiation

The UO_2 electrode was placed in a Pyrex glass-lined pressure vessel (Hastelloy C) with 1 L capacity containing 0.1 mol L^{-1} NaCl solution (310 cm³) prepared with purified H_2O. The pH of the solution was adjusted to 9.5 using a NaOH solution. A large surface area Pt mesh counter electrode and Ag/AgCl (0.1 mol L^{-1} KCl) reference electrode, custom-designed to withstand the elevated pressures imposed, were used. The potential of the reference electrode was measured before and after each experiment against an SCE electrode (used only as a standard) and found to be between −0.034 V and −0.042 V. Potentials were converted to the SCE scale to facilitate comparison to electrochemical measurements. All experiments were conducted at 22 ± 1 °C.

The pressure vessel was placed in the irradiation chamber of the lead-lined gamma cell. The chamber was equipped with a sealed ^{192}Ir γ-source with a half life of 74 d and an initial activity of 10^7 Ci provided by MDS Nordion, Kanata, Ontario. This source could be remotely introduced into, and removed from, the irradiation chamber. When in the chamber, the source was located directly beneath the pressure vessel. Dosimetry performed before and after the series of experiments showed all irradiated experiments were performed within the dose rate range 15.9 Gy h^{-1} to 11.3 Gy h^{-1}.

The pressure vessel was purged with high-purity Ar gas at atmospheric pressure to deaerate the solution prior to electrochemical measurements. During experiments, the pressure vessel was filled with either Ar or H_2 gas at a pressure of 5.2 MPa. In some irradiated experiments, the gas in the pressure vessel was switched from Ar to H_2, or vice versa, while irradiation was continued. The gas line was designed to avoid the possibility of contamination by atmospheric O_2 or residual H_2 when switching from H_2 to Ar atmospheres during irradiation. However, it was possible minor amounts of H_2 absorbed in the Hastelloy C autoclave may have been released when switching H_2 to Ar atmospheres. Before each experiment, the electrode was cathodically cleaned at −1.3 V$_{SCE}$ for 5 min

3. Results and discussion

3.1. Electrode characterization

Both the Dy-UO_2 and $UO_{2.002}$ electrodes have been well characterized. Energy dispersive X-ray analyses confirmed that the Dy^{III} dopant

was homogeneously distributed throughout the matrix [33]. Raman analyses detected no peaks indicating the presence of Dy_2O_3, consistent with the Dy^{III} cations being in solid solution. Current sensing atomic force microscopy showed a slight unevenness in the distribution of non-stoichiometric sites on the $UO_{2.002}$ surface, suggesting they were primarily located in grain boundary locations [34].

The reactivity of the Dy-UO_2 electrode was shown to be considerably lower than that of the $UO_{2.002}$ electrode [34] with anodic dissolution not detected until a potential of ~0.1 V (vs SCE). By contrast dissolution could be detected at potentials $\leq$ −0.5 V (vs SCE) on $UO_{2.002}$. Since the thermodynamic threshold for the oxidation of stoichiometric UO_2 is ~ −0.4 V (vs SCE) under our experimental conditions, this indicated a slight degree of sub-thermodynamic oxidation of the $UO_{2.002}$ (i.e., oxidation at a potential lower than expected for $UO_{2.000}$) allowing the dissolution of non-stoichiometric locations. This enhanced reactivity with increased non-stoichiometry has been demonstrated using scanning electrochemical microscopy [30,35]. Based on Raman spectroscopic analyses, the matrix stabilization induced by RE^{III} (Dy^{III}) doping was attributed to the influence of RE^{III}-O_V clustering where O_V are the oxygen vacancies in the UO_2 fluorite lattice [36]. The formation of these clusters decreased the availability of the vacancies required to accommodate the injection of interstitial (O_I) during oxidation.

The UO_2 used in radiation experiments was not as well characterized, although, as standard CANDU reactor fuel, it was expected to be close to stoichiometric. However, voltammetric experiments have shown that sub-thermodynamic oxidation could occur if the original reductive sintering during pellet fabrication was incomplete [11].

X-ray photoelectron spectroscopic measurements have shown that the anodic dissolution of UO_2, irrespective of whether it was doped or not, was preceded by the formation of a thin (3–5 nm) oxidized surface layer (Eq. 1),

$$U^{IV}O_2 \rightarrow U^{IV}_{1-2x}U^{V}_{2x}O_{2+x} \tag{1}$$
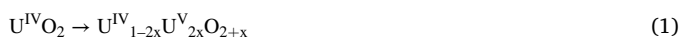
with the extent of oxidation (i.e., x) increasing with potential [31, 37]. Fig. 1 shows the relationship between the extent of oxidation, defined by the ratio of oxidized states ($U^V + U^{VI}$) to the total U ($U^{IV} + U^V + U^{VI}$), and applied potential calculated from previously published data [37]. These analyses were performed on Gd-doped UO_2 which has been shown to exhibit a very similar reactivity to Dy-UO_2. A similar dependence of composition on E_{CORR} has been observed on UO_2 surfaces corroded in H_2O_2 [38]. These relationships indicate that the potential, whether applied or achieved on open circuit (i.e., at E_{CORR}), is an indication of the surface composition over the potential range from ~ −0.4
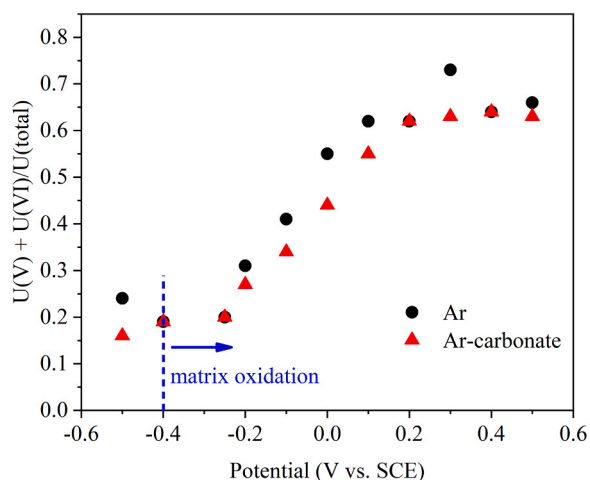
V (vs SCE) to ~0.2 V (vs SCE).

When HCO_3^-/CO_3^{2-} was present, the oxidized surface states were effectively U^V with negligible amounts of U^{VI} which was soluble as carbonate complexes, $U^{VI}O_2(CO_3)_x^{(2-2x)+}$. Consequently, the ratio is a measure of the extent of oxidation to yield the thin $U^{IV}_{1-2x}U^{V}_{2x}O_{2+x}$ layer via reaction 1. In the absence of HCO_3^-/CO_3^{2-}, a minor, but increasing, amount of U^{VI} was retained on the surface as the applied potential was increased accounting for the slightly increased ratio at positive potentials. As discussed elsewhere [31], the decrease in the ratio at the most positive potential in the absence of HCO_3^-/CO_3^{2-} can be attributed to enhanced dissolution of U^{VI} states due to local acidification caused by the hydrolysis of dissolved $U^{VI}O_2^{2+}$. In the present study, this relationship between composition and potential (from ~−0.4 V (vs SCE) to ~0.2 V (vs SCE)) was used as a template for the extent of oxidation of the electrode surfaces.

3.2. The influence of surface pre-treatment on UO_2 oxidation

Fig. 2 shows the influence of a cathodic treatment on the electrochemical behavior of both the Dy-UO_2 and $UO_{2.002}$ electrodes. If a potential of −0.6 V (vs SCE) was applied immediately after immersion in the solution, both electrodes exhibited a small negative current which rapidly decreased to a negligible value over the first ~ 20 s. For both electrodes, if a more negative pretreatment potential (E_{PRE}) of −1.2 V (vs SCE) was first applied, a negative current due to the reduction of H_2O was observed (not shown) which switched to a positive current and decayed with time when the potential was subsequently reduced to −0.6 V (vs SCE), Fig. 2.

These results suggested that, as H^+ (from H_2O) was reduced (at −1.2 V), the UO_2 surface was also reduced, leading to the need for an
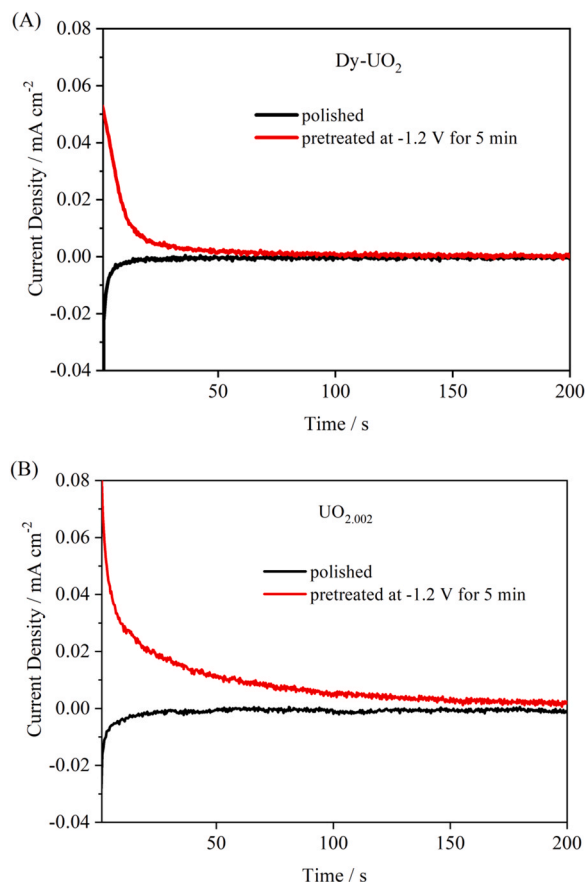
(A)

Dy-UO_2

— polished
— pretreated at -1.2 V for 5 min

(B)

$UO_{2.002}$

— polished
— pretreated at -1.2 V for 5 min

Fig. 2. *Potentiostatic current-time curves recorded on the Dy-UO_2 (A) and $UO_{2.002}$ (B) electrodes at −0.6 V (vs SCE) in Ar-purged 0.1 mol L^{-1} NaCl, pH = 9.8.*

Fig. 1. *Comparison of $(U^V + U^{VI})/U_{total}$ ratio as a function of potential measured on a Gd-UO_2 electrode in Ar purged 0.1 mol L^{-1} NaCl with and without HCO_3^-/CO_3^{2-} (0.05 mol L^{-1}) [37]. The vertical dashed line indicates the thermodynamic threshold for oxidation of the UO_2 matrix in carbonate-free solution.*

anodic re-oxidation when the applied potential was decreased to -0.6 V (vs SCE), a potential at which H_2O reduction was no longer possible. This latter potential (-0.6 V) was also below the thermodynamic threshold for the oxidation of a stoichiometric UO_2 matrix (-0.4 V (vs SCE), Fig. 1), confirming that the anodic current can only be attributed to the re-oxidation of reduced species produced at -1.2 V (vs SCE), not further oxidation of the UO_2 matrix.

Fig. 3 shows the influence of E_{PRE} on the subsequent voltammetric behavior recorded on Dy-UO_2 (A) and $UO_{2.002}$ (B). The vertical marker indicates the thermodynamic threshold above which the anodic oxidation of the UO_2 matrix (reaction 1) could occur, accompanied by an increasing extent of oxidative dissolution as $U^{VI}O_2(OH)_y^{(2-y)+}$ and the deposition of $U^{VI}O_3 \cdot zH_2O$ as the potential was increased. For both electrodes, while the potential was held at E_{PRE}, the negative current for H_2O reduction remained approximately constant and increased as E_{PRE} was made more negative with the values of the current effectively the same on both electrodes for all three E_{PRE} values.

For the Dy-UO_2 electrode, after applying -1.2 V (vs SCE) for 5 min, only a minor anodic current was observed in the sub-thermodynamic range on the subsequent anodic scan, with the current increasing for potentials positive to the threshold, indicating the onset of the anodic formation of the $U^{IV}_{1-2x}U^V_{2x}O_{2+x}$ layer. On the reverse scan, the shallow negative current observed in the potential range -0.4 V (vs SCE) to -1.1 V (vs SCE) has been shown to be due to the reduction of the products of matrix oxidation formed on the forward scan [34]. When E_{PRE} was made more negative, leading to an increase in the reduction current for H_2O (not shown), the positive current in the

sub-thermodynamic region increased markedly with the current in the matrix oxidation region also increasing. Despite this increase in matrix oxidation current at potentials greater than the thermodynamic threshold, the current on the reverse scan for the reduction of matrix oxidation products (-0.4 to -1.1 V) decreased, indicating that the enhanced current on the anodic scan could not be attributed to enhanced matrix oxidation, but was due to re-oxidation of the surface reduced at E_{PRE}. The lack of matrix oxidation at potentials positive to the thermodynamic threshold despite the observation of a positive current, suggested the matrix re-oxidation was incomplete and further oxidation of the matrix by reaction 1 inhibited.

For the $UO_{2.002}$ electrode, the CV appeared tilted, an indication that the considerably higher resistance of this electrode (> 2 kΩ) was not fully compensated. Despite this, the general features of the anodic and cathodic processes were visible. When $E_{PRE} = -1.2$ V (vs SCE), a very shallow oxidation process was observed on the forward scan at potentials below the thermodynamic threshold. This can be attributed to enhanced oxidation at the non-stoichiometric locations shown to exist in this electrode. On the reverse scan, the reduction of the anodically oxidized matrix (at potentials > -0.2 V (vs SCE)) was observed, as expected, as shallow currents in the potential range -0.4 V (vs SCE) to -0.9 V (vs SCE). Applying more negative values of E_{PRE} had an almost negligible effect on the subsequent voltammetric behavior, Fig. 3B, despite the fact that the cathodic currents for H_2O reduction were effectively the same on this electrode as on the Dy-UO_2 electrode.

If the influence of Dy^{III} doping of UO_2 was to achieve charge balance by the creation of an equivalent number of U^V sites, the composition of the Dy-UO_2 electrode would be $U^{IV}_{0.648}U^V_{0.176}Dy^{III}_{0.176}O_2$, compared to $U^{IV}_{0.996}U^V_{0.004}O_{2.002}$ for the $UO_{2.002}$ electrode. This suggested the application of an E_{PRE} value sufficiently negative to reduce H_2O to H_2 simultaneously reduced U^V in the matrix, a process which would be observable on the heavily doped Dy-UO_2, but not on the close-to-stoichiometric $UO_{2.002}$. The observation of a large sub-thermodynamic re-oxidation process on the subsequent voltammetric scan on the Dy-UO_2 electrode could then be attributed to the re-establishment of the charge-balanced Dy-UO_2 matrix by re-oxidation of the reduced U^V states. That this re-oxidation led to a suppression of the matrix oxidation process at potentials higher than the thermodynamic limit (-0.4 V (vs SCE)), despite a high current at higher potentials, suggested the complete re-oxidation of the reduced matrix was incomplete on the time frame of the voltammetric scan.

Fig. 4 shows CVs recorded on the Dy-UO_2 electrode in solutions with different pH values. Prior to recording the voltammetric scans, an $E_{PRE} = -1.2$ V (vs SCE) was applied for 5 min. For pH values of 10 and 5, only a minor anodic current was observed in the sub-thermodynamic potential range (< -0.4 V (vs SCE)) when the potential was scanned to more positive values, indicating that no major matrix reduction occurred at E_{PRE}. For the two lower pH values, re-oxidation did occur with the re-oxidation current increasing as the pH was decreased from 4 to 3. This indicated that, for matrix reduction ($U^V \rightarrow U^{IV}$) to occur, a significant current for H^+ reduction was required, the application of E_{PRE} being insufficient on its own. This requirement suggested the processes were linked with reduction of H^+ to $H\bullet$, leading to the subsequent reduction of U^V in the oxide matrix.

The observation that H_2O and U^V reduction occurred simultaneously suggested that the $H\bullet$ radicals produced by H_2O reduction could be responsible for the reduction of U^V. The $H\bullet$ created electrochemically on the surface, would be expected to be mobile within the matrix [39]. Since they were also highly reducing, they would have reduced the U^V states with the H^+ produced maintaining charge balance without the need to eject O^{II} ions from the matrix. On the subsequent anodic scan, Figs. 3 and 4, the re-oxidation of these reduced U states would then account for the observed anodic currents. This reduction/re-oxidation process would be expected to become more extensive as the value of E_{PRE} was reduced from -1.2 V (vs SCE) to -1.5 V (vs SCE), as observed in Fig. 3A, since the rate of production of $H\bullet$ by H_2O reduction would be
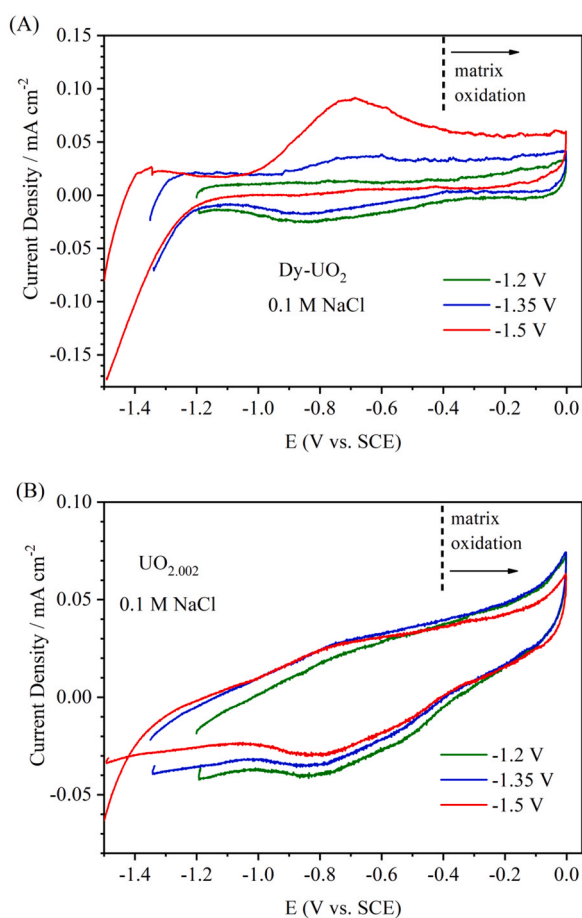
Fig. 3. *CVs recorded on the Dy-UO_2 (A) and $UO_{2.002}$ (B) electrodes in an Ar-purged 0.1 mol L^{-1} NaCl, pH = 10.0. The scan rate = 10 mV s^{-1}. Before each measurement, the electrode was cathodically treated at E_{PRE} (-1.2 V, -1.35 V or -1.5 V) for 5 min.*
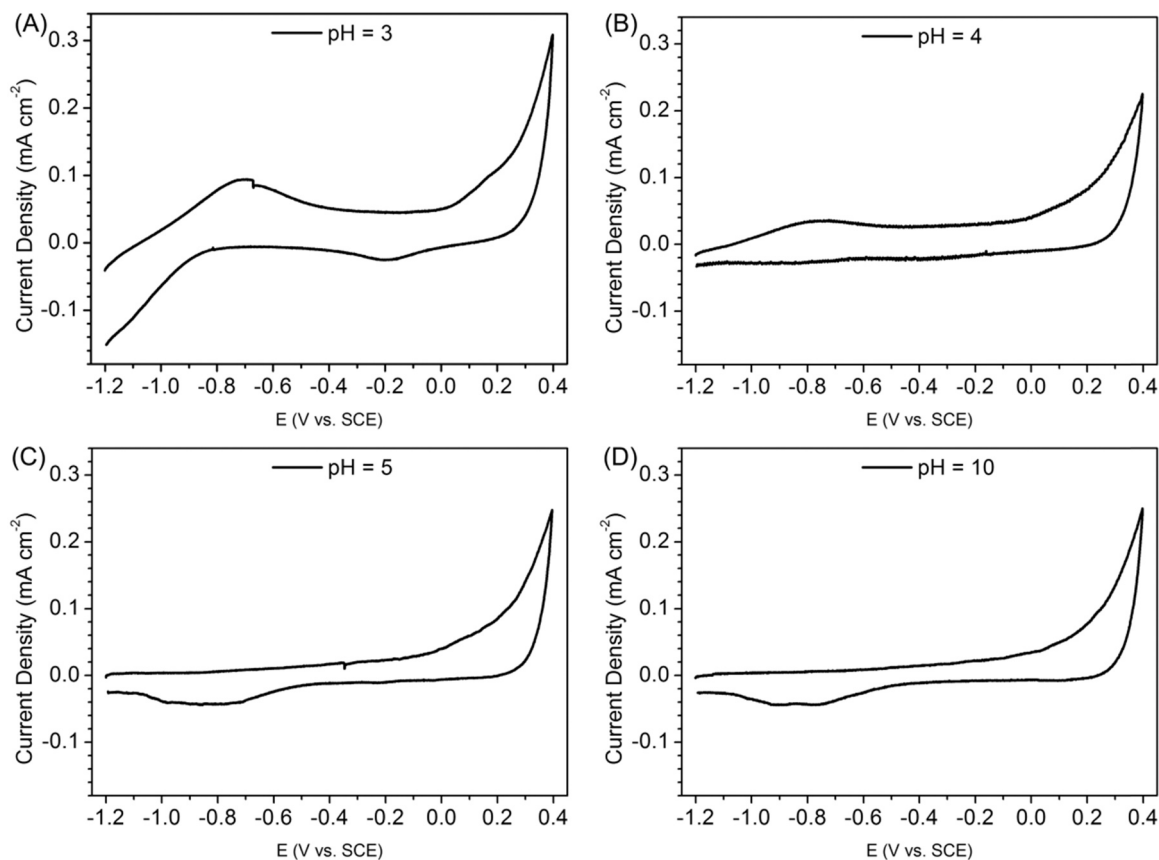
Fig. 4. *CVs recorded on the Dy-UO$_2$ electrode in an Ar-purged 0.1 mol L^{-1} NaCl solution with different pH values. The scan rate = 10 mV s^{-1}. Before each measurement, the electrode was polished and cathodically treated at E$_{PRE}$ = −1.2 V for 5 min.*

increased. By contrast, reduction and re-oxidation would be only minor processes on UO$_{2.002}$ for which the U^V content was very low, as observed in Fig. 3B.

3.3. The influence of surface pre-treatment on E$_{CORR}$

Fig. 5 shows the influence of E$_{PRE}$ on E$_{CORR}$ for the Dy-UO$_2$ (Fig. 5A) and UO$_{2.002}$ (Fig. 5B) electrodes. In these experiments 0.001 M HCO$_3^-$/CO$_3^{2-}$ was added to the solution to avoid the accumulation of U^{VI}O$_3$•zH$_2$O, due to corrosion by residual O$_2$ in the Ar-purged solution over the ~40 h open circuit exposure. For the polished, but cathodically untreated electrodes, the values of E$_{CORR}$ were in the range −0.3 V (vs SCE) to −0.4 V (vs SCE). Location of these values on the calibration plot in Fig. 1 showed that the residual oxidation of the surface was minor although the increase in E$_{CORR}$ at longer exposure times (> 200 min) suggested some oxidation of the UO$_2$ surface was inevitable.

After applying negative potentials (E$_{PRE}$ = −1.2 V or −1.5 V), E$_{CORR}$ was considerably more negative on first switching to open circuit, but increased exponentially with time approaching the value for the untreated electrode, thus demonstrating that the matrix reduction process enforced at E$_{PRE}$ was reversible. While not a rate parameter which could yield information on the extent of reaction, E$_{CORR}$ reflected the relative rates of the anodic and cathodic reactions occurring on the surface of the electrode. The form of the recovery profile was different for the two electrodes. For the UO$_{2.002}$, E$_{CORR}$ recovered slowly with time over a 500 min period but was almost independent of the value of E$_{PRE}$. This electrode had a very low U^V content located predominantly at grain boundaries, making reduced U^V states non-uniformly distributed in the electrode surface. Since both the amount of available H$^+$ and the number of reduced sites requiring re-oxidation would have decreased with time on open circuit, the increase in E$_{CORR}$ was a qualitative indication that

the interfacial rate was decreasing. Eventually, the recovery in E$_{CORR}$ was complete (i.e., the value measured on the untreated electrode was achieved) and exceeded the thermodynamic threshold indicating matrix oxidation by reaction with dissolved O$_2$ had occurred.

In contrast, for the Dy-UO$_2$ electrode with a high and uniformly distributed U^V content, the recovery of E$_{CORR}$ was dependent on the value of E$_{PRE}$, and did not indicate a complete recovery, never reaching the value observed on the non-reduced surface, Fig. 5A. For E$_{PRE}$ = −1.5 V (vs SCE), a slight shoulder in E$_{CORR}$ was observed prior to the exponential increase. Although not visible on the scale of Fig. 5A, a similar shorter transition was observed after reduction at E$_{PRE}$ = −1.2 V (vs SCE). This contrast with the behavior observed on UO$_{2.002}$ reflected the differences in U^V content and distribution. The reduction of the large number of uniformly distributed U^V states would produce a uniformly distributed reduced surface layer. The slow initial arrest in E$_{CORR}$ could then be attributed to the kinetically controlled re-oxidation of this outer layer before the need for transport of H$^+$ to the surface to support the interfacial reaction initiating the exponential increase. As indicated by the differences in current in the CVs for the two electrodes, Fig. 3, the extent of the reduced matrix reoxidation process was much greater on the Dy-UO$_2$ electrode than on the UO$_{2.002}$ electrode.

3.4. The influence of γ radiation on E$_{CORR}$ in the presence of dissolved H$_2$

Fig. 6 shows the evolution of E$_{CORR}$ in γ-irradiated solution purged with either Ar or over-pressured with 5 MPa of H$_2$. Here only representative plots are shown. In these experiments the electrode was initially polarized to −1.3 V (vs SCE) to remove air-formed oxides from the surface. In unirradiated solutions, there was no significant difference in the steady-state E$_{CORR}$ values measured in Ar or H$_2$ atmospheres, with values falling within the range −0.37 V (vs SCE) and −0.42 V (vs SCE)
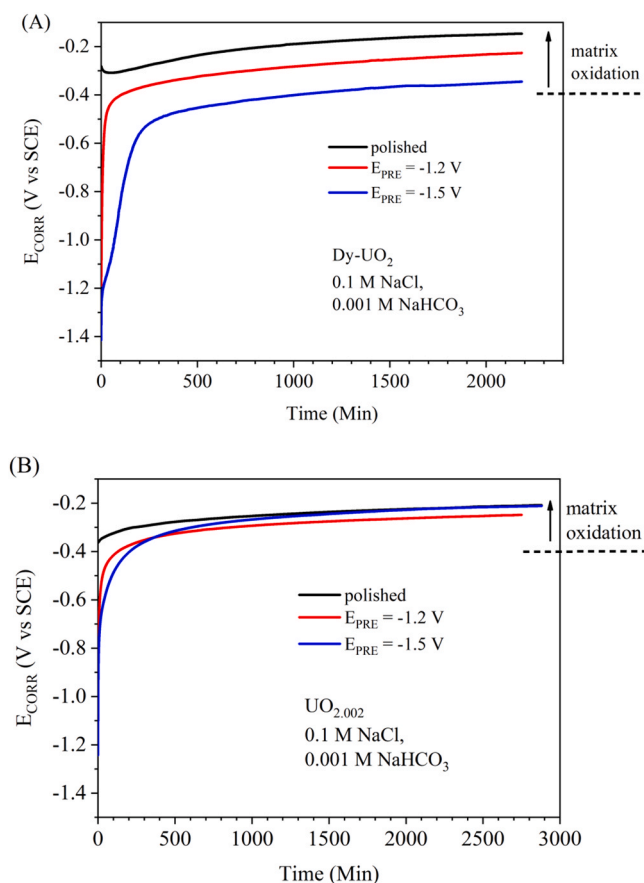
Fig. 5. *Corrosion potential (E_{CORR}) measured on the Dy-UO$_2$ (A) and UO$_{2.002}$ (B) electrodes in Ar-purged 0.1 mol L^{-1} NaCl with 0.001 mol L^{-1} NaHCO$_3$, pH = 8.0. The electrodes were pretreated by polishing or at different values of E_{PRE} for 5 min.*
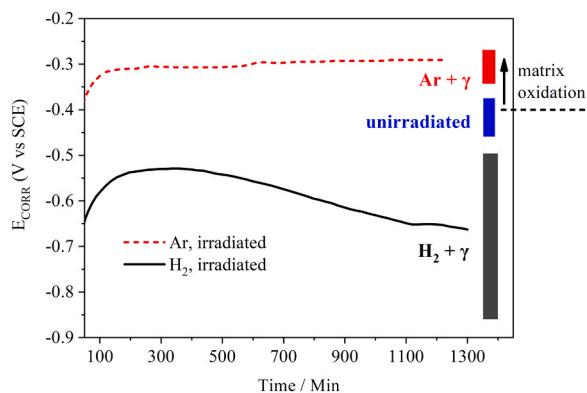

Fig. 6. *The corrosion potential (E_{CORR}) of UO$_2$ in γ-irradiated 0.1 mol L^{-1} NaCl at room temperature in the presence of 5.2 MPa H$_2$ or Ar. The range of final E_{CORR} values measured in a series of irradiated solutions containing either H$_2$ or Ar are shown as the black and red vertical bar, respectively. The range of E_{CORR} values in unirradiated solutions containing either Ar or H$_2$ is shown as the blue vertical bar.*
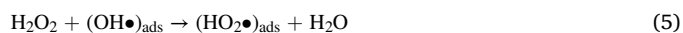
(i.e., around the thermodynamic threshold), as indicated by the vertical blue bar in Fig. 6. In Ar-purged solutions in the presence of radiation (Ar + γ), E_{CORR} increased achieving steady-state values in the range −0.35 V (vs SCE) to −0.27 V (vs SCE) as indicated by the red bar in the figure. This range of values was above the thermodynamic threshold, with location of these values on the profile in Fig. 1 indicating slight oxidation of the UO$_2$ surface via reaction 1.

Since γ radiation produces a mixture of oxidants and reductants, this

increase in E_{CORR} indicated a dominant influence of oxidants with reaction involving radical species [10,16,40,41],

$$U^{IV} + H_2O_2 \rightarrow U^V + (OH\bullet)_{ads} + OH^- \quad (2)$$

$$U^{IV} + (OH\bullet)_{ads} \rightarrow U^V + OH^- \quad (3)$$

Slight oxidation by H$_2$O$_2$ (via the radicals it produces) has been shown to catalyze H$_2$O$_2$ decomposition [1], a process which also proceeds via a radical mechanism [40–42],

$$H_2O_2 \rightarrow 2(OH\bullet)_{ads} \quad (4)$$

$$H_2O_2 + (OH\bullet)_{ads} \rightarrow (HO_2\bullet)_{ads} + H_2O \quad (5)$$

$$2(HO_2\bullet)_{ads} \rightarrow H_2O_2 + O_2 \quad (6)$$

The establishment of a steady-state value of E_{CORR} in the range −0.35 V (vs SCE) to −0.27 V (vs SCE) and, hence, a slightly oxidized steady-state surface composition (Fig. 1), was consistent with the predominance of H$_2$O$_2$ decomposition since catalysis would be achieved by the reversible interconversion of U^{IV}/U^V surface sites [1]. The irreversible oxidation of the UO$_2$ surface has been shown to require a potential ($\geq$ −0.2 V (vs SCE)), beyond which tetragonal distortions of the cubic UO$_2$ lattice led to irreversible oxidation and the onset of matrix breakdown [34]. This appeared to occur once the composition exceeded U$^{IV}_{0.7}$U$^V_{0.3}$O$_{2.15}$, a threshold identified by Raman spectroscopy [43], and consistent with Fig. 1.

When H$_2$ was present with radiation (H$_2$ + γ), γ-radiation could split H$_2$ into (H•)$_{ads}$ (reaction 7). Since γ-radiolysis of H$_2$O produces H$_2$O$_2$, (OH•)$_{ads}$ can be formed via reaction 4, and (H•)$_{ads}$ can be produced by reaction 8. Fig. 6 showed that E_{CORR} initially increased before eventually decreasing to more negative values. A series of similar experiments (not shown) [44] showed that while the form of the E_{CORR} transients was reproducible the absolute values of E_{CORR} varied significantly, as indicated by the range of values observed after 1300 min (indicated by the black bar in Fig. 6). The form of the transients suggested the initial rapid oxidation of UO$_2$ by reactions 2 and 3 was reversed, at least in part by the ability of H$_2$ to scavenge radiolytic oxidants, via the interaction of H• with adsorbed OH• (reaction 9), a process well known in radiolysis studies [16,45].

$$H_2 + \gamma \rightarrow 2(H\bullet)_{ads} \quad (7)$$

$$H_2 + (OH\bullet)_{ads} \rightarrow H_2O + (H\bullet)_{ads} \quad (8)$$

$$(H\bullet)_{ads} + (OH\bullet)_{ads} \rightarrow H_2O \quad (9)$$

However, if this was the only influence of H$_2$ + γ, then E_{CORR} would be expected to stabilize at a value within the range measured under unirradiated conditions, indicated by the vertical blue bar in Fig. 6. The enforced decrease in E_{CORR} at longer exposure times suggested H$_2$ was exerting a distinct influence on the surface composition as observed when H$_2$O/H$^+$ reduction was electrochemically driven on the UO$_2$ surface (Fig. 5).

Additional evidence for a direct influence of H$_2$ + γ on the surface composition is shown in Fig. 7 for experiments in which the pressurized gas in the cell was switched, in the presence of radiation, between Ar and H$_2$. When the switch was from Ar to H$_2$, E_{CORR} began to decrease immediately, indicating that the radiolysis process sustaining surface oxidation was quickly suppressed by the radiation-induced activation of H$_2$, at least at the H$_2$ pressure and dose rate employed in this study. E_{CORR} eventually achieved a value below the thermodynamic threshold for oxidation of the UO$_2$ matrix. This indicated a reduction of the UO$_2$ matrix, whose resistivity indicated a significant level of non-stoichiometry (Section 2.1.1), by H atoms similar to that achieved electrochemically. Since the eventual E_{CORR} was below the threshold for matrix oxidation it was possible further reduction of U^{IV} to U^{III} occurred, although this could not be demonstrated in this study.

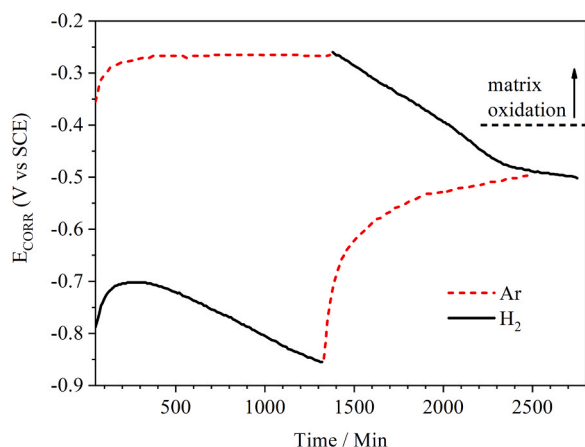That this matrix reduction process was reversible was demonstrated

Fig. 7. *The evolution of E_{CORR} on UO_2 when the pressurizing gas was changed between Ar and H_2 in γ-irradiated 0.1 mol L^{-1} NaCl solution at room temperature.*

in experiments in which the surface was first reduced by exposure to γ + H_2 and then the purge gas switched to Ar while irradiation was continued, Fig. 7. On switching to Ar the decrease in E_{CORR} was reversed with E_{CORR} increasing exponentially towards the thermodynamic threshold of −0.4 V (vs SCE). This behavior was similar to that observed electrochemically when E_{PRE} (at which H_2O reduction to H• occurred) was switched off and E_{CORR} allowed to recover. As suggested electrochemically, the exponential increase in E_{CORR} could be attributed to the diffusion of H^+ within the oxide matrix to the surface prior to its reduction in support of the re-oxidation of the surface. It is noteworthy that the trend in E_{CORR} was towards the thermodynamic threshold, with the slightly oxidizing conditions which prevailed in the absence of radiation not re-established. This suggested the reductive influence of H_2 + γ might not have been fully reversible with the radiolytic oxidizing effect suppressed, at least within the time frame and at the γ dose rates employed in this study.

A similar suppression of E_{CORR} by dissolved H_2 has been reported in the absence of radiation [23,46] on SIMFUELs [7,47], with the dissociation of H_2 to H• radicals, catalyzed on noble metal particles, leading to a suppression of the oxidation of the UO_2 matrix. Fig. 8 shows the effect of increasing H_2 pressure on the E_{CORR} measured on SIMFUEL in neutral 0.1 M KCl at 60 °C. The value of E_{CORR} decreased with increasing H_2 pressure approaching a value close to the calculated equilibrium potential for the H^+/H_2 redox reaction, indicating that E_{CORR} was
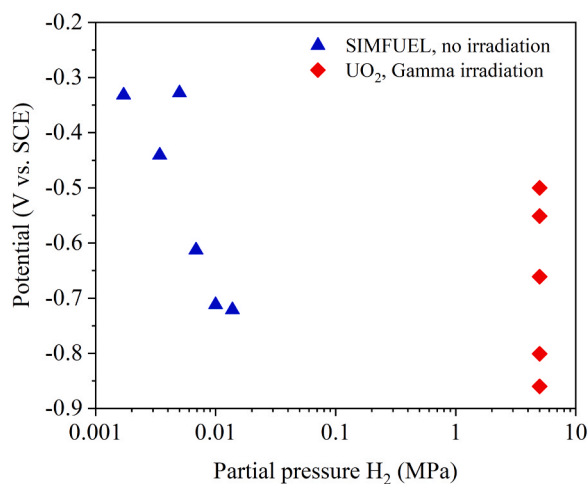
dictated by the kinetics of this redox reaction. The range of E_{CORR} values in the present study, conducted at a significantly higher H_2 pressure in the presence of radiation, also, in some cases, were in the proximity of the H^+/H_2 equilibrium potential value, consistent with an approach to a similar redox equilibrium on the UO_2 surface in the absence of noble metal particles to that observed on SIMFUELs [7,47].

3.5. Comparison of electrochemical and irradiation behavior and its relevance to nuclear waste disposal

The similarity in the response of E_{CORR} to both electrochemical polarization and exposure to an irradiated solution pressurized with H_2 suggests that the mechanism leading to reduction of the UO_2 matrix is the same in both cases. As illustrated schematically in Fig. 9A, the application of a negative potential leads to the reduction of U^V states in the matrix to U^{IV}. While this reduction could occur by a direct electrochemical reaction, this pathway is minor compared to the indirect reaction involving the formation of H atoms and their transport into the matrix leading to its reduction. It is this second indirect reduction reaction which occurs in the H_2 + γ solution, with the H atoms produced radiolytically, as indicated schematically in Fig. 9B.

These results demonstrates that the combination of γ-radiation and H_2 leads to the reduction of the U^V states in the UO_2 matrix, which protect the UO_2 from corrosion since the formation of a $U^{IV}_{1-2x}U^V_{2x}O_{2+x}$ layer (reaction 1) is the initial step in the overall oxidative dissolution (corrosion) process. This offers an explanation for the many published observations that a combination of radiation and dissolved H_2 suppresses UO_2 corrosion [10,19,22–24,26–29]. There is also some evidence in this study that this combination leads to the irreversible reduction of the matrix rendering it unreactive if H_2, but not the radiation field, is subsequently removed, although the available evidence is
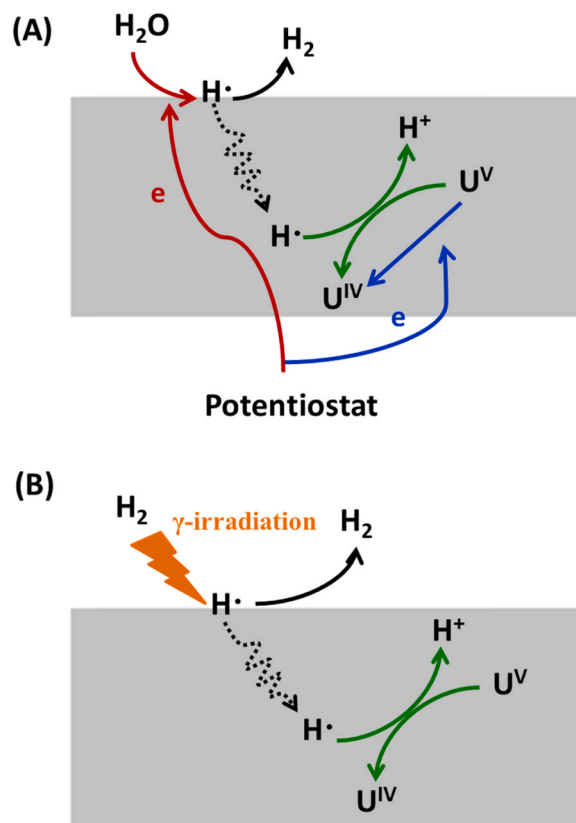

Fig. 9. *Schematic illustration comparing the proposed mechanisms for the electrochemical (A) and radiolytic (B) reduction of U^V states within a doped or nonstoichiometric UO_2 matrix.*

Fig. 8. *Summary of corrosion potential (E_{CORR}) values of SIMFUEL [19] in the presence of H_2 in 0.1 mol L^{-1} KCl at 60 °C, and UO_2 in γ-irradiated 0.1 mol L^{-1} NaCl at room temperature in the presence of 5.2 MPa H_2 (this work).*

not conclusive.

From the perspective of the behavior of spent nuclear fuel within a failed waste container emplaced in a DGR, these results indicate that, while radiolytic oxidants will be produced by H_2O radiolysis within a water-containing container, their ability to drive fuel corrosion and the release of radionuclides would be suppressed by the copious production of H_2 by corrosion of the steel vessel. While the reactivity of H_2 could be stimulated by its activation on noble metal particles in the fuel, activation could also be achieved on the fuel surface when γ radiation is present. It is likely that a similar activation could be achieved in the presence of α radiation although this remains to be demonstrated.

4. Summary and conclusions

(1) The electrochemical reduction of UO_2 specimens containing different amounts of U^V has been compared. Providing the applied potential was sufficiently negative that H_2O/H^+ reduction could occur, the U^V states in the oxide were reduced by H atoms, formed electrochemically on the oxide surface, which diffuse into the matrix and were reoxidized to H^+.

(2) The extent of reduction was determined by the U^V content of the oxide and the rate of production of H atoms.

(3) When the electrode was subsequently switched to open circuit, this process was reversed with H^+ transport to the electrode surface leading to its reduction back to H_2 and reoxidation of the lattice. This process was followed by monitoring the E_{CORR}.

(4) In the presence of a combination of γ radiation and dissolved H_2, the E_{CORR} was suppressed to negative values indicating a similar reduction of the U^V states in the UO_2 matrix to that induced electrochemically. That this suppression was driven by the radiolytic dissociation of H_2 to H atoms was demonstrated by switching the purge gas from H_2 to Ar while maintaining the radiation field, when the relaxation in E_{CORR} exhibited similar behavior to that observed after electrochemical polarization.

(5) This demonstrated that the influence of H atoms produced radiolytically was the same as those produced electrochemically.

(6) This comparison identifies a mechanism by which H_2 could suppress the oxidation of spent nuclear fuel inside a failed waste container in a DGR.

CRediT authorship contribution statement

Nazhen Liu: Investigation, Writing – original draft. **Fraser King:** Investigation, Writing – review & editing. **James J. Noël:** Writing – review & editing, Supervision. **David W. Shoesmith:** Writing – review & editing, Supervision, Project administration.

Declaration of Competing Interest

The authors declare that they have no known competing financial interests or personal relationships that could have appeared to influence the work reported in this paper.

Data availability

The raw/processed data required to reproduce these findings cannot be shared at this time due to technical or time limitations.

Acknowledgements

References

[1] Z. Zhu, J.J. Noël, D.W. Shoesmith, Hydrogen peroxide decomposition on simulated nuclear fuel bicarbonate/carbonate solutions, Electrochim. Acta 340 (2020) 135980–135990.

[2] J. Chen, M. Behazin, J. Binns, K. Birch, A. Blyth, S. Briggs, J. Freire-Canosa, G. Cheema, R. Crowe, D. Doyle, F. Garisto, J. Giallonardo, M. Gobien, R. Guo, S. Hirschorn, M. Hobbs, M. Ion, J. Jacyk, H. Kasani, P. Keech, E. Kremer, C. Lawrence, H. Leung, K. Liberda, T. Liyanage, J. McKelvie, C. Medri, M. Mielcarek, L. Kennell-Morrison, A. Murchison, A. Parmenter, M. Sanchez-Rico Castejon, U. Stahmer, Y. Sui, E. Sykes, M. Sykes, T. Yang, X. Zhang, B. Zhao. Technical Program for Long-term Management of Canada's Used Nuclear Fuel – Annual Report 2018, NWMO-TR-2019-01, Nuclear Waste Management Organization,, Toronto, Ontario, 2019.

[3] N. Liu, Z. Zhu, L. Wu, Z. Qin, J.J. Noël, D.W. Shoesmith, Predicting radionuclide release rates from spent nuclear fuel inside a failed waste disposal container using a finite element model, Corrosion 75 (3) (2019) 302–308.

[4] N. Liu, Z. Zhu, J.J. Noël, D.W. Shoesmith, Corrosion of nuclear fuel inside a failed waste container, in: K. Wandelt (Ed.), Encyclopedia of Interfacial Chemistry, vol. 6, Surface Science and Electrochemistry, 2018, pp. 172–182.

[5] N. Liu, Z. Qin, J.J. Noël, D.W. Shoesmith, Modelling the radiolytic corrosion of α-doped UO2 and spent nuclear fuel, J. Nucl. Mater. 494 (2017) 87–94.

[6] N. Liu, L. Wu, Z. Qin, D.W. Shoesmith, Roles of radiolytic and externally generated H2 in the corrosion of fractured spent nuclear fuel, Environ. Sci. Technol. 50 (2016) 12348–12355.

[7] P.G. Lucuta, R.A. Verrall, Hj Matzke, B.J. Palmer, Microstructural features of SIMFUEL-simulated high-burnup UO2-based nuclear fuel, J. Nucl. Mater. 178 (1991) 48–60.

[8] Z. Zhu, L. Wu, J.J. Noël, D.W. Shoesmith, Anodic reactions occurring on simulated spent nuclear fuel (SIMFUEL) in hydrogen peroxide solutions containing bicarbonate/carbonate – the effect of fission products, Electrochim. Acta 320 (2019) 134546–134556.

[9] L. Wu, Z. Qin, D.W. Shoesmith, An improved model for the corrosion of used nuclear fuel inside a failed waste container under permanent disposal conditions, Corros. Sci. 84 (2014) 85–95.

[10] J.C. Wren, D.W. Shoesmith, S. Sunder, Corrosion behavior of uranium dioxide in Alpha radiolytically decomposed water, J. Electrochem. Soc. 152 (11) (2005) B470–-B4481.

[11] D.W. Shoesmith, Fuel corrosion processes under waste disposal conditions, J. Nucl. Mater. 282 (2000) 1–31.

[12] E. Ekeroth, O. Roth, M. Jonsson, The relative impact of radiolysis products in radiation induced oxidative dissolution of UO2, J. Nucl. Mater. 355 (2006) 38–46.

[13] D.W. Shoesmith. Used Fuel and Uranium Dioxide Dissolution Studies – a Review, NWMO TR-2007-03, Nuclear Waste Management Organization,, Toronto, Ontario, 2007.

[14] H. He, M. Broczkowski, K. O'Neil, D. Ofori, O. Semenikhin, D. Shoesmith. Corrosion of Nuclear Fuel (UO2) Inside a Failed Nuclear Waste Container, NWMO TR-2012-09, Nuclear Waste Management Organization,, Toronto, Ontario, 2012.

[15] D.W. Shoesmith, The chemistry/electrochemistry of spent nuclear fuel as a wasteform, in: P. Burns, G. Simon (Eds.), Uranium: Cradle to Grave, 43, Mineralogical Society of Canada, Short Course Series, 2013, pp. 337–368.

[16] T.E. Eriksen, D.W. Shoesmith, M. Jonsson, Radiation induced dissolution of UO2 based nuclear fuel – a critical review of predictive modelling approaches, J. Nucl. Mater. 420 (2012) 409–423.

[17] D.W. Shoesmith, J.J. Noel, Z. Qin, C.T. Lee, J.S. Goldik, B.G. Santos, M. E. Broczkowski. Corrosion of Nuclear Fuel (UO2) Inside a Failed Waste Container, 06819-REP-01200-10145-R00, Ontario Power Generation,, Toronto, Ontario, 2005.

[18] L. Wu, Y. Beauregard, Z. Qin, S. Rohani, D.W. Shoesmith, A model for the influence of steel corrosion products on nuclear fuel corrosion under permanent disposal conditions, Corros. Sci. 61 (2012) 83–91.

[19] M.E. Broczkowski, D. Zagidulin, D.W. Shoesmith, The role of dissolved hydrogen on the corrosion/dissolution of spent nuclear fuel. Nuclear Energy and the Environment, American Chemical Society Symposium,, Washington, DC, 2010, pp. 349–380.

[20] J. Bruno, K. Spahiu, The long-term effect of hydrogen on the UO2 spent fuel stability under anoxic conditions: findings from the Cigar Lake Natural Analogue study, Appl. Geochem. 49 (2014) 178–183.

[21] K. Spahiu, J. Devoy, D. Cui, M. Lundström, The reduction of U (VI) by near field hydrogen in the presence of UO2 (s), Radiochim. Acta 92 (2004) 597–601.

[22] M.E. Broczkowski, P.G. Keech, J.J. Noël, D.W. Shoesmith, The role of dissolved hydrogen on rare earth – doped uranium dioxide corrosion in the presence of hydrogen peroxide, J. Electrochem. Soc. 158 (12) (2011) C439–-C444.

[23] M.E. Broczkowski, J.J. Noël, D.W. Shoesmith, The inhibiting effects of hydrogen on the corrosion of uranium dioxide under nuclear waste disposal conditions, J. Nucl. Mater. 346 (2005) 16–23.

[24] M.E. Broczkowski, P.G. Keech, J.J. Noël, D.W. Shoesmith, Corrosion of uranium dioxide containing simulated fission products in dilute hydrogen peroxide and dissolved hydrogen, J. Electrochem. Soc. 157 (8) (2010) C275–-C281.

[25] J.K. Noerskov, T. Bligaard, A. Logadottir, J.R. Kitchin, J.G. Chen, S. Pandelov, U. Stimming, Trends in the exchange current for hydrogen evolution, J. Electrochem. Soc. 152 (2005) J23–J26.

[26] P. Carbol, J. Cobos-Sabate, J.-P. Glatz, C. Ronchi, V. Rondinella, D.H. Wegen, T. Wiss, A. Loida, V. Metz, B. Kienzler, K. Spahiu, B. Grambow, J. Quinones, A. Martinez Esparza Valiente. The Effect of Dissolved Hydrogen on the Dissolution

of 233U doped UO2(s), High Burn-up Spent Fuel and MOX Fuel, TR-05-09, Swedish Nuclear Fuel and Waste Management Company,, Stockholm, 2005.

[27] T. Eriksen, M. Jonsson. The Effect of Hydrogen on Dissolution of Spent fuel in 0.01 mol×dm–3 NaHCO3 Solution, TR-07-06, Swedish Nuclear Fuel and Waste Management Company,, Stockholm, 2007.

[28] D.W. Shoesmith. The Role of Dissolved Hydrogen on the Corrosion/Dissolution of Spent Nuclear Fuel, NWMO-TR-2008-19, Nuclear Waste Management Organization,, Toronto, Ontario, 2008.

[29] M.E. Broczkowski, J.J. Noël, D.W. Shoesmith, The influence of dissolved hydrogen on the surface composition of doped uranium dioxide under aqueous corrosion conditions, J. Electroanal. Chem. 602 (2007) 8–16.

[30] H. He, R.K. Zhu, Z. Qin, P.G. Keech, Z. Ding, D.W. Shoesmith, Determination of local corrosion kinetics on hyper-stoichiometric UO_{2+x} by scanning electrochemical microscopy, J. Electrochem. Soc. 156 (3) (2009) C87–C94.

[31] B.G. Santos, H.W. Nesbitt, J.J. Noël, D.W. Shoesmith, X-ray photoelectron spectroscopy study of anodically oxidized SIMFUEL surfaces, Electrochim. Acta 49 (2004) 1863–1873.

[32] F. King, M.J. Quinn, N.H. Miller. The Effect of Hydrogen and Gamma Radiation on the Oxidation of UO2 in 0.1M NaCl Solution, TR-99-27, Swedish Nuclear Fuel and Waste Management Company,, Solna, 1999.

[33] M. Razdan, D.W. Shoesmith, Influence of trivalent-dopants on the structural and electrochemical properties of uranium dioxide (UO_2), J. Electrochem. Soc. 161 (3) (2014) H105–-H113.

[34] N. Liu, H. He, J.J. Noel, D.W. Shoesmith, The electrochemical study of Dy_2O_3 doped UO_2 in slightly alkaline sodium carbonate/bicarbonate and phosphate solutions, Electrochim. Acta 235 (2017) 654–663.

[35] H. He, Z. Qin, D.W. Shoesmith, Characterizing the relationship between hyperstoichiometry, defect structure and local corrosion kinetics of uranium dioxide, Electrochim. Acta 56 (2010) 53–60.

[36] H. He, P.G. Keech, M.E. Broczkowski, J.J. Noël, D.W. Shoesmith, Characterization of the influence of fission product doping on the anodic reactivity of uranium dioxide, Can. J. Chem. 85 (2007) 702–713.

[37] M. Razdan, D.W. Shoesmith, The electrochemical reactivity of 6.0 wt% Gd-doped UO_2 in aqueous carbonate/bicarbonate solutions, J. Electrochem. Soc. 161 (4) (2014) H225–H234.

[38] M. Razdan, D.W. Shoesmith, The influence of hydrogen peroxide and hydrogen on the corrosion of simulated spent nuclear fuel, Faraday Discuss. 180 (2015) 283–299.

[39] S.B. Emery, E.G. Sorte, R.C. Bowman Jr., Z.Z. Fang, C. Ren, E.H. Majzoub, M. S. Conradi, Detection of fluorite-structured MgD_2/TiD_2: deuterium NMR, J. Phys. Chem. C 119 (2015) 7656–7661.

[40] C.M. Lousada, A.J. Johansson, T. Brinck, M. Jonsson, Mechanism of H_2O_2 decomposition on transition metal oxide surfaces, J. Phys. Chem. C 116 (2012) 9533–9543.

[41] A. Barreiro Fidalgo, B. Dahlgren, T. Brinck, M. Jonsson, Surface reactions of H_2O_2, H_2, and O_2 in aqueous systems containing ZrO_2, J. Phys. Chem. C 120 (2016) 1609–1614.

[42] C.M. Lousada, M. Yang, K. Nilsson, M. Jonsson, Catalytic decomposition of hydrogen peroxide on transition metal and lanthanide oxides, J. Mol. Catal. A 379 (2013) 178–184.

[43] H. He, D.W. Shoesmith, Raman spectroscopic studies of defect structures and phase transition in hyper-stoichiometric UO_{2+x}, Phys. Chem. Chem. Phys. 12 (2010) 8108–8117.

[44] F. King, D.W. Shoesmith. Electrochemical Studies of the Effect of H2 on UO2 Dissolution, TR-04-20, Swedish Nuclear Fuel and Waste Management Company,, Stockholm, 2004.

[45] B. Pastina, J. Isabey, B. Hickel, The influence of water chemistry on the radiolysis of the primary coolant water in pressurized water reactors, J. Nucl. Mater. 264 (1999) 309–318.

[46] M. Broczkowski. The Effects of Hydrogen and Temperature on the Electrochemistry and Corrosion of Uranium Dioxide, University of Western Ontario,, London, Canada, 2008. PhD Thesis.

[47] A.F. Gerwing, F.E. Doern, W.H. Hocking, X-Ray photoelectron spectroscopy on radioactive materials using a McPherson ESCA-36 equipped with an SSL position-sensitive detector, Surf. Interface Anal. 14 (1989) 559–566.